Allosteric Spin-Crossover induced by Ligand-Based Molecular Alloying

Carlos Bartual-Murgui,*[,†,¬] Cristian Pérez-Padilla,[†] Simon Teat,[§] Oliver Roubeau*[,#] and Guillem Aromí*[,†,‡]

[†] Departament de Química Inorgànica i Orgànica, Universitat de Barcelona, Diagonal 645, 08028 Barcelona, Spain. E-mail: aromi@ub.edu

[#] Instituto de Ciencia de Materiales de Aragón (ICMA), CSIC and Universidad de Zaragoza, Pedro Cerbuna 12, 50009, Zaragoza, Spain.

[‡] Institute of Nanoscience and Nanotechnology of the University of Barcelona (IN2UB), Barcelona, Spain.

KEYWORDS Spin-Crossover, magnetism, Single Crystal X-ray Diffraction, Molecular Alloying, Cooperativity.

Supporting Information Placeholder

ABSTRACT: The spin crossover (SCO) molecular material $[Fe(Mebpp)_2](ClO_4)_2$ (**2**) has been doped with increasing amounts of the ligand Me2bpp (Mebpp and Me2bpp = methyl and bis-methyl substituted bis-pyrazolylpyridine ligands) yielding molecular alloys with formula $[Fe(Mebpp)_{2-2x}(Me2bpp)_{2x}](ClO_4)_2$ (**4***x*; $0.05 < x < 0.5$). Alloys with up to seven different compositions have been studied through single crystal X-ray diffraction (SCXRD), magnetometry and differential scanning calorimetry (DSC). The decrease of cooperativity of the spin transition and the variation of its critical temperature have been studied in light of precise molecular structures. A SCO process occurring as a result of an allosteric effect has been unveiled.

INTRODUCTION

Spin Crossover (SCO) compounds are a very intensely studied family of molecular materials.[1-4] They are made of transition metals able to display two different distributions with similar energy of their *d* electrons and thus to lie easily in two distinct spin states (low and high spin; LS and HS). Therefore, one can shuttle reversibly between one another by employing external stimuli (light, thermal, pressure or chemical environment changes, etc.). Since both states exhibit different magnetic as well as other physical properties, SCO systems are very promising as potential molecular switches for the construction of nanoscopic functional devices.[5,6] In this context, Fe(II) is the most exploited ion,[7-9] since it can toggle between a non-magnetic (LS; S=0) and a magnetic (HS; S=2) state, undergoing significant changes to optical, dielectric, structural and other properties. The structural changes result from differences of around 10% in Fe–L (L = ligand donor atom) distances between both states. These are at the root of important structural effects associated to the spin-state switching,[10] such as crystallographic phase transitions[11] or symmetry breaking.[12-14] Also, the propagation of these changes through the crystal lattice by elastic interactions is at the origin of cooperativity,[15] which is the essential requirement to observe bistability.[16] The latter is another key feature of potential switchable functional materials, therefore, important efforts are devoted to establish precise relationships between structure and cooperativity with a view of predicting or mastering its effects.[17] Attempts to assess the impact of intermolecular interactions on cooperativity involve the investigation of families of SCO compounds varying systematically some lattice component, such as counter-ions[18-22] or solvent molecules of crystallization.[23-31] Series of analogous complexes systematically changing the periphery of the ligands have been studied as well.[30,32-36] Another approach targets the preparation of various polymorphs of SCO compounds,[11,37-40] thus keeping the exact same composition while changing the crystallographic arrangement of the components. Differences to the spin switching properties originate in these cases exclusively from the crystal lattice. All the above studies base their conclusions on the effect of replacing one entire crystallographic lattice by another. There is a more subtle procedure, consisting on gradually replacing one component from the crystal network and observe the impact of this progressive substitution on the temperature, completeness and abruptness of the SCO.[41,42] This method allows to focus on specific aspects defining the cooperativity as well as the temperature of the transition. Most efforts have focused on doping the crystal lattice of Fe(II) SCO complexes with isostructural species of non-switching M(II) metals (Zn, Ni, Mn, Co or Cd). Here, the insertion of species that do not undergo a spin transition, interrupts the propagation of the structural changes of the SCO, thus diminishing the cooperativity.[43-51] This metal dilution also affects the amount of residual HS or LS species at the lower or higher temperature regions, respectively. More specifically, using metals with $r(M^{2+})>r(Fe^{2+})$ stabilizes the HS state whereas metals with $r(M^{2+})<r(Fe^{2+})$ favors the LS of Fe^{2+}, as a result of a "negative" and "positive" chemical pressure, respectively.[52,53] The SCO temperature suffers a decrease upon dilution as well,[47,48,54-67] which has been modelled quantifying the change in HS to LS free energy differences caused by the changes in elastic interactions within the lattice with the varying composition. The doping approach, also termed molecular alloying, has been used only very rarely when the variable component is a ligand of the SCO complex rather than the metal. This variation affects the intermolecular interactions within the lattice while not diminishing the number of potential SCO centers. Therefore, the variable of internal pressure is expected to play a different role in the analysis here than with the mixed-metal systems. A pioneering achievement was that of reducing the temperature of the wide hysteresis of the 1D polymeric compound $[Fe(Htrz)_3](ClO_4)_2$ (Htrz=1,2,4-triazole; ΔT = 17 K, centered at 304.5 K) to convenient values by ligand-

based molecular alloying. The ligand 4-amino-1,2,4-triazole (4-NH_2trz), similar to that of the original material, was introduced randomly into the parent system thus generating solid solutions of coordination chains with composition $[Fe(Htrz)_{3-3x}(4\text{-}NH_2trz)_{3x}](ClO_4)_2$.[68] Since the other pure polymer $[Fe(4\text{-}NH_2trz)_3](ClO_4)_2$ undergoes a gradual SCO at 130 K, it was found that ligand-based alloys in the $0 < x < 0.1$ range exhibit hysteresis loops centered at the temperatures given by $T(x) = 304.5 - 170x$. The doping of the ligand also causes a reduction of the hysteresis width ($\Delta T(x) = 17 - 20x$ K). This system was later analyzed for all possible compositions ($0 < x < 1$), which allowed to refine the numerical dependences with x, while a thermodynamic model was proposed based on the existence of alloys made of mixtures of two different 1D chains. More recently, an analogous study was performed on the coordination polymer $[Fe(btzx)_3](ClO_4)_2$ (btzx = 1,4-bis(tetrazol-1-yl)-*p*-xylene), with the progressive substitution of btzx by the structurally related ligand 1,4-bis(triazol-1-yl)-*p*-xylene (btix). This produced mixtures of the alloy $[Fe(btzx)_{3-3x}(btix)_{3x}](ClO_4)_2$ that was more accurately described as chains with a statistical and random distribution of both bridging ligands for each composition (as given by x). The solid solutions exhibit a different magnetic behavior than both pure compounds, with the appearance of additional SCO events. The alloy is maintained only until $x \approx 0.5$. Beyond this composition, the separation of the pure phase $[Fe(btix)_3](ClO_4)_2$ is observed. To the best of our knowledge, ligand-based molecular alloying on discrete SCO complexes has not been performed yet. We recently reported a method to obtain two polymorphs of the molecular SCO material $[Fe(bpp)_2](ClO_4)_2$ (**1**; bpp=2-(pyrazol-1-yl)-6-(pyrazol-3-yl)pyridine).[37] These two polymorphs, **1**α and **1**β, crystallize in two different space groups ($P2_1/c$ and $P2_1/n$, respectively) and exhibit abrupt SCO with a very narrow hysteresis, centered at 277 and 315 K respectively, with quite different cooperativity. In addition, we prepared the derivatives $[Fe(Mebpp)_2](ClO_4)_2$ (**2**) and $[Fe(Me2bpp)_2](ClO_4)_2$ (**3**) using the methyl functionalized ligands (Scheme 1) 2-(3-methyl-pyrazol-1-yl)-6-(pyrazol-3-yl)pyridine (Mebpp) and 2-(3,5-dimethyl-pyrazol-1-yl)-6-(pyrazol-3-yl)pyridine (Me2bpp).[69] Interestingly, these complexes (Fig. 1) are arranged in the crystal lattice as polymorphs **1**α and **1**β, respectively (Fig. S1).

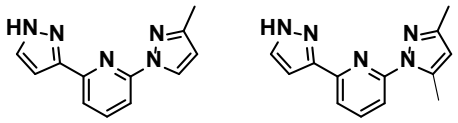

Scheme 1. Ligands Mebpp and Me2bpp.

The magnetic properties of **2** and **3** are certainly influenced by the crystal packing but strongly affected by the presence of methyl groups at positions 5 and/or 3 of the pyrazol-1-yl ring for steric reasons. They thus exhibit an abrupt SCO at $T_{SCO} = 184$ and 378 K, respectively.[69] In this work, we take advantage of the structural similarity between the complexes of **2** and **3** to undertake a study of molecular alloying by introducing gradually increased fractions of ligand Me2bpp to the reaction conducing to complex **2**, thus producing solid solutions of composition $[Fe(Mebpp)_{2-2x}(Me2bpp)_{2x}](ClO_4)_2$ (**4***x*; $0.05 < x < 0.5$). The influence of this dilution to the SCO temperature and the cooperativity is analyzed *via* extensive single crystal X-ray diffraction (SCXRD), as well as mass spectrometry (MS), magnetic susceptibility measurements and differential scanning calorimetry (DSC). At all dilutions, the SCO is found to be complete in one sole conversion for both components, thus unveiling an allosteric effect.

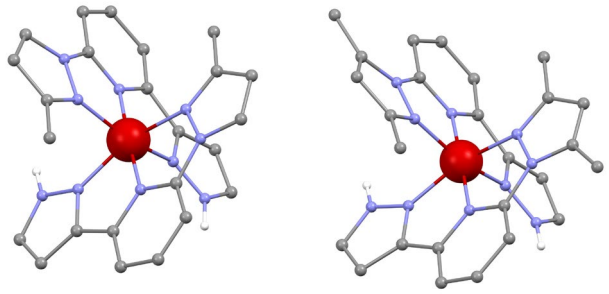

Figure 1. Representation of the molecular structure of the complex cations of $[Fe(Mebpp)_2](ClO_4)_2$ (**2**, left) and $[Fe(Me2bpp)_2](ClO_4)_2$ (**3**, right). Red, Fe; gray, C; purple, N; white, H. Only hydrogen atoms from N−H moieties shown.

EXPERIMENTAL

Synthesis

Ligands 2-(3-methyl-pyrazol-1-yl)-6-(pyrazol-3-yl)pyridine (Mebpp) and 2-(3,5-dimethyl-pyrazol-1-yl)-6-(pyrazol-3-yl)pyridine (Me2bpp), as well as complexes $[Fe(Mebpp)_2](ClO_4)_2$ (**2**) and $[Fe(Me2bpp)_2](ClO_4)_2$ (**3**) were prepared as previously published.[69] **Caution:** Perchlorate salts of metal complexes are potentially explosive. Only small quantities of material should be prepared, and the samples should be handled with care.

$[Fe(Mebpp)_{2-2x}(Me2bpp)_{2x}](ClO_4)_2$ (4*x*; 0.05 < *x* < 0.5). To solutions of $Fe(ClO_4)_2 \cdot 6H_2O$ (0.023 g, 0.065 mmol) and ascorbic acid (□2 mg) in absolute ethanol (10 mL) were added dropwise solutions of Mebpp (0.027(1−*x*) g, 0.12(1−*x*) mmol) and Me2bpp (0.029*x* g, 0.12*x* mmol) in absolute ethanol (10 mL). The resulting dark yellow solutions were stirred for 40 minutes at room temperature. The solutions were then filtered and layered with Et_2O (1:1 vol.). Yellow crystals of the products suitable for single crystal X-ray diffraction were obtained as homogeneous phases, after approximately 4 days. Typical yields: ~40%. EA (%), calcd (found) for $Fe(C_{12}H_{11}N_5)_{1.2}(C_{13}H_{13}N_5)_{0.8}(ClO_4)_2$ (*x*=0.4): C, 41.61 (41.45); H, 3.32 (3.34); N, 19.58 (19.07). $Fe(C_{12}H_{11}N_5)_{1.6}(C_{13}H_{13}N_5)_{0.4}(ClO_4)_2$ (*x*=0.2): C, 41.26 (40.59); H, 3.24 (3.21); N, 19.73 (19.14). $Fe(C_{12}H_{11}N_5)_{1.8}(C_{13}H_{13}N_5)_{0.2}(ClO_4)_2$ (*x*=0.1): C, 41.08 (40.96); H, 3.19 (3.14); N, 19.81 (19.48). $Fe(C_{12}H_{11}N_5)_{1.9}(C_{13}H_{13}N_5)_{0.1}(ClO_4)_2$ (*x*=0.05): C, 41.00 (40.60); H, 3.17 (3.14); N, 19.85 (19.41). ESI MS: *m/z* = 505.2 ($[Fe(Mebpp)_2]-[H^+]^+$, 519.2 ($[Fe(Mebpp)(Me2bpp)]-[H^+]^+$, 533.2 ($[Fe(Me2bpp)_2]-[H^+]^+$, 605.11 ($[Fe(Mebpp)_2](ClO_4)-2[H^+]^+$, 619.13 ($[Fe(Mebpp)(Me2bpp)](ClO_4)-2[H^+]^+$, 633.14 ($[Fe(Me2bpp)](ClO_4)-2[H^+]^+$.

Single-crystal X-ray diffraction (SCXRD)

Data for the series **4***x* were acquired at 100 K on either a Bruker APEXII QUAZAR diffractometer equipped with a microfocus multilayer monochromator with MoKα radiation ($\lambda = 0.71073$ Å, x = 0.15), or on a Bruker APEX II CCD diffractometer at the Advanced Light Source beam-line 11.3.1 at Lawrence Berkeley National Laboratory, from a silicon 111 monochromator (λ = 0.77490 Å, all other compounds). The temperature dependence of the cell parameters was obtained on the same setups. Data reduction and absorption corrections were performed with respectively SAINT and SADABS.[70] All structures were solved by intrinsic phasing with SHELXT[71] and refined by full-matrix least-squares on F^2 with SHELXL-2014.[72] All details can be found in CCDC **XXXX-XXXX** that contain the supplementary crystallographic data for this paper. These data can be obtained free of charge from The Cambridge Crystallographic Data Center via https://summary.ccdc.cam.ac.uk/structure-summary-form. Crystallographic and refinement parameters are summarized in Table S1 together with average Fe–N bond lengths and distortion pa-

rameters. Selected bond lengths and angles and intermolecular distances are given in Tables S2 to S4.

Physical Measurements

The elemental analysis was performed with an elemental microanalyzer (A5), model Flash 1112, at the Servei de Microanàlisi of CSIC, Barcelona, Spain. IR spectra were recorded on KBr pellet samples on a Nicolet AVATAR 330 FTIR spectrometer. MALDI-TOF mass spectrometry measurements were performed on a 400 ABSciex MALDI-TOF spectrometer at the Unitat d'Espectrometria de Masses de Caracterització Molecular (CCiT) of the University of Barcelona. Samples were prepared as follows: 5 µL of the solution were diluted in 5 mL of MeOH. Then, 0.5 µL of internal reference solution, containing 10 mg/mL of DCTB in dichloromethane, were added before injection.

Magnetic measurements were performed with either a MPMS5 or MPMS-XL SQUID magnetometer respectively through the "Unitat de mesures Magnètiques" of the Universitat de Barcelona or the "Servicio General de Apoyo a la Investigación-SAI", Universidad de Zaragoza. Corrections of the diamagnetic contributions of the sample holder and the sample were applied.

Differential Scanning Calorimetry (DSC) was carried out at a scanning rate of 10 $Kmin^{-1}$ with a Q1000 calorimeter from TA Instruments equipped with the LNCS accessory. Temperature and enthalpy scales were calibrated with the melting transition of a standard sample of In (156.6 °C, 3296 $Jmol^{-1}$). Mechanically crimped Al pans with an empty pan as a reference were used. A synthetic sapphire was measured in the same temperature range to derive heat capacity. By comparison, an overall accuracy of 0.2 K for the temperature and up to 10% for the heat capacity was estimated.

RESULTS AND DISCUSSION

Synthesis and Mass Spectrometry

The series of compounds $[Fe(Mebpp)_{2-2x}(Me2bpp)_{2x}](ClO_4)_2$ (**4***x*; $0.05 < x < 0.5$) was prepared through reactions in ethanol of $Fe(ClO_4)_2 \cdot 6H_2O$ with Mebpp/Me_2bpp mixtures of the appropriate composition, following the layering of the resulting solutions in Et_2O, in the same manner as reported for **2** and **3**.[69] Homogeneous phases of good quality single crystals were obtained for the compositions with $x = 0.05, 0.1, 0.15, 0.2, 0.3, 0.4, 0.5$. For compositions with $x > 0.5$, it was not possible to obtain single phases. Instead, crystals of **3** and of molecular alloys of the **4***x* type (*vide infra*) were obtained. This clearly indicates that systems with $x > 0.5$ cannot be accommodated as solid solutions in the crystal lattice **1***α* (that of compounds **4***x*, for $0.05 < x < 0.5$, and of **2**, where $x = 0$; Fig. S1).

The reaction mixtures were analyzed after 30 minutes of stirring, by mass spectrometry. The crystals later isolated from all these systems were dissolved and analyzed as well. All the spectra exhibit three prominent peaks corresponding to the three possible fragments of Fe(II) coordinated to two bpp ligands (Fig. S2), namely, $([Fe(Mebpp)_2]-[H^+])^+$ (*m/z* = 505.2), $([Fe(Mebpp)(Me2bpp)]-[H^+])^+$ (*m/z* = 519.2) and $[Fe(Me2bpp)_2]-[H^+])^+$ (*m/z* = 533.2). While the relative intensity of the heteroleptic species increases as *x* approaches 0.5, the presence of the three fragments in all the diagrams suggests that the former is not specially favored and the distribution of ligands among the complex cations may be close to statistical. In each case, the composition is maintained upon crystallization since the results from the initial solutions are almost the same as these from the dissolved single crystals for almost all the compositions studied (Fig S3).

Single Crystal X-Ray Diffraction

SCXRD data were collected on single crystals of $[Fe(Mebpp)_{2-2x}(Me2bpp)_{2x}](ClO_4)_2$ (**4***x*) with several compositions ($x = 0.05$, 0.1, 0.15, 0.2, 0.3, 0.4, 0.5) at 100 K. All compounds crystallize in the monoclinic space group *C2/c*, the same as complex **2**. The composition revealed by the refined models of these data is indeed consistent with solid solutions as formulated for **4***x*. Thus, in all cases, the asymmetric unit (Fig. 2) is solvent free and composed by one $[Fe(Mebpp)_{2-2x}(Me2bpp)_{2x}]^{2+}$ cation in addition to two ClO_4^{2-} anions to ensure electroneutrality. The latter are forming hydrogen bonds to the N–H groups of the complex cation. This cation features an Fe(II) center chelated by two approximately perpendicular tridentate bpp ligands, yielding a distorted octahedral geometry. The identity of each of these ligands is Mebpp or Me2bpp, distributed randomly among all the complexes of the lattice in the proportion given by *x*. The distributions at both ligand positions can be distinguished on basis of residual electron density at the corresponding atom sites, and are not identical. The specific composition reported at each ligand position (Table 1) reflects on the occupancies of the 5–methyl substituent of Me2bpp (C25 and C12) that optimize their displacement parameters, the ensemble satisfying the composition given by *x*.

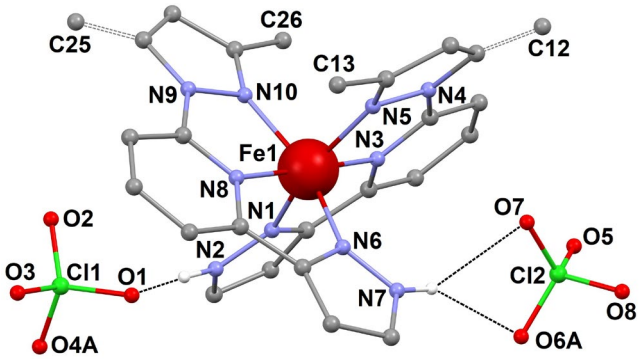

Figure 2. Representation of a molecular structure representative of the molecular alloys $[Fe(Mebpp)_{2-2x}(Me2bpp)_{2x}](ClO_4)_2$ (**4***x*), here for $x = 0.5$. The C-atoms of the partially occupied methyl groups of Me2bpp (C12 and C25) are shown linked to the pyrazolyl ring with dashed bonds. Black dashed lines are hydrogen bonds. Only hydrogen atoms from N−H moieties shown.

The presence of the partially occupied 5-methyl substituents into the alloy engenders disorder to the ClO_4^- anions, which becomes more apparent for $x = 0.1$ or larger. Slightly different chemical environments at both sites originate the occupation disparities between C12 and C25. The average Fe–N distances across the series span the 1.962 to 1.966 Å range, indicating that the metal centers lie in the LS state at 100 K. The molecular structure was also determined at 220 K for $x = 0.01$ and at 280 K for $x = 0.3$ and 0.15. The essential features of the structures at higher temperatures are approximately the same as described above for the systems measured at 100 K. The most significant quantitative change is an increase of the Fe–N bond distances by approximately an 8%, amounting to 2.126 Å in average. This denotes that the Fe(II) ions have undergone a SCO transition to the HS state (see below). The organization within the lattice of the components of the $[Fe(Mebpp)_{2-2x}(Me2bpp)_{2x}](ClO_4)_2$ systems is analogous for all the structures analyzed. The complexes are disposed in parallel sheets, which are in turn approximately perpendicular to the bpp ligands (Fig. 3), thus to the N_{py}–Fe–N_{py} axes (N_{py} = N donors of the pyridyl fragment of bpp).

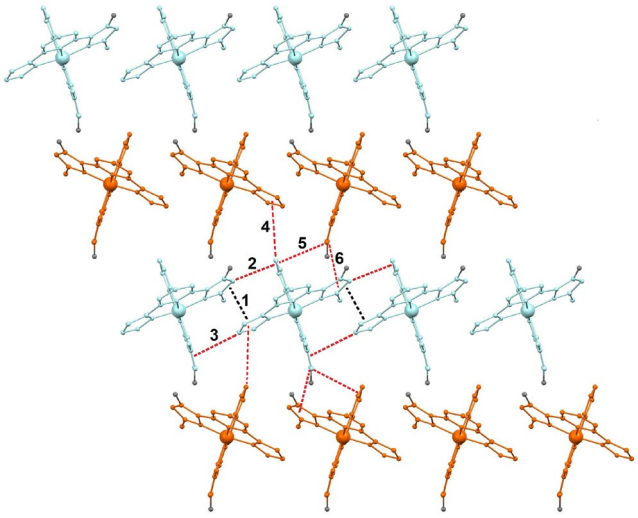

Figure 3. Sheet organization of the cations in all **4***x* compounds, emphasizing their two different orientations and the relevant π···π (black dashed) and C–H···π (red dashed) interactions formed by each complex with its first neighbours within the sheet. The crystallographic independent interactions are labelled 1 to 6.

Table 1. Relevant parameters[(a)] of the structure and SCO of compounds **2** (x=0), $[Fe(Mebpp)_{2-2x}(Me2bpp)_{2x}](ClO_4)_2$ (**4***x*) and **3** (x=1).

x	C12[a] (%)	C25[a] (%)	"contact 5" (Å)	$\Delta\beta$ (º)	T_{SCO} (K)	ΔT_{80} (K)	Γ/RT_{SCO}	$T_{\pi\varepsilon\alpha\kappa}$ (K)	$\Delta_{SCO}H$ (kJmol^{-1})	$\Delta_{SCO}S$ (Jmol^{-1}K^{-1})	n^{Sorai}	T^{Sorai} (K)
0 (**2**)	N/A	N/A	3.061	2.58	184.0	16.7	2.01	183.1	5.87	31.74	21.34	185.6
0.05	5	5	3.088	2.41	184.4	36.5	1.92	184.7	4.94	26.32	15.90	185.8
0.1	5	15	3.135	2.13	187.5	57.4	1.70	188.1	4.85	25.09	9.41	190.3
0.15	12	18		1.79	190.3	87.3	1.57	-	-	-	-	-
0.2	17	23	3.153	1.79	193.6	92.9	1.49	194.4	3.65	18.16	7.01	199.8
0.3	25	35	3.195	1.55	198.4	106.8	1.39	201.9	3.50	17.08	5.89	208.5
0.4	35	45	3.273	1.19	207.3	120.4	1.36	209.8	2.99	14.10	5.85	218.9
0.5	37	63	3.470	1.10	226.3	119.9	1.33	244.4	3.29	15.12	5.78	225.1
1 (**3**)	N/A	N/A	N/A	-	381.1	70.0	1.70	375.2	14.11	37.98	9.0(1)	375.0(3)

[a] C12 and C25 are the occupancies of the 5–methyl substituent from Me2bpp at each ligand position; contact 5 is the intermolecular contact that suffers the largest variations with increased x (see Fig. 3 and SI); $\Delta\beta$ is the total variation of the monoclinic cell angle β over the SCO temperature range; the SCO characteristic temperature T_{SCO} is defined as the temperature at which half of the Fe centers have undergone the transition (*i.e.* HS fraction γ_{HS} = 0.5); ΔT_{80} is the temperature range over which 80% of the SCO is completed; Γ is the measure of the SCO cooperativeness derived through the regular solution model (see SI);[73] T_{peak}, $\Delta_{SCO}H$ and $\Delta_{SCO}S$ are the peak temperature, excess enthalpy and entropy associated with the SCO anomaly in heat capacity data; n^{Sorai} and T^{Sorai} are the domain size and SCO temperature derived through Sorai's domain model (see SI).[74,75]

Within these sheets, the $[Fe(Mebpp)_{2-2x}(Me2bpp)_{2x}]^{2+}$ species feature two different orientations, as observed in polymorph **1***α* of complex **1** and in complex **2**, but not **3**. The latter exhibits the same lattice as polymorph **1***β* (Fig. S1). Therefore, the lattice of **2** is capable to accommodate increasing amounts of ligand Me2bpp up to $x \approx 0.5$. Upon reaching this limit, mixtures of crystals of different phases are obtained, indicating that the lattice of **1***α* does not admit larger concentrations of the doping ligand. The composition changes are mirrored by gradual variations in metric parameters. In Fig. 4 are shown variations to the cell volume (up to 3.7%), to the cell parameter a and to the unit cell angle β, at 100 K. This is also translated into a gradual variation of the distances defining the main intermolecular interactions (see below).

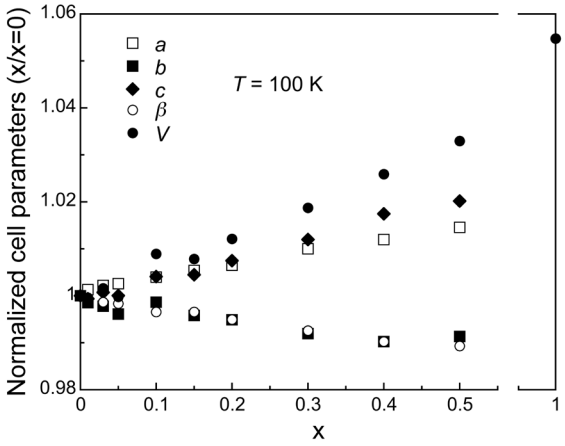

Figure 4. Relative variation of the crystallographic unit cell parameters and volume with the value of x in the structures of the $[Fe(Mebpp)_{2-2x}(Me2bpp)_{2x}](ClO_4)_2$ (**4***x*) compounds at 100 K.

Magnetic and Thermal Signatures of SCO and its Cooperativity

The effect of doping complex **2** with increasing amounts of Me2bpp on the magnetic properties of the resulting alloys was analyzed through variable temperature magnetic susceptibility measurements (Fig. 5). The solid solutions $[Fe(Mebpp)_{2-2x}(Me2bpp)_{2x}](ClO_4)_2$ (**4***x*) with x = 0.05, 0.1, 0.15, 0.2, 0.3, 0.4 and 0.5 were analyzed under a constant magnetic field of 1T in between 2 and 300 K (or 360 K) in the warming and cooling modes, both giving superimposable data for each studied value of x. In Fig. 5 are represented $\chi_M T$ *vs* T plots (χ_M is the molar paramagnetic susceptibility per Fe^{2+} center for each compound). Pure complex **2**, $[Fe(Mebpp)_2](ClO_4)_2$, was previously reported to exhibit an abrupt, almost complete SCO process with T_{SCO} = 184 K.[69] Growing proportions of Me2bpp render the SCO curves more gradual while T_{SCO} increases progressively (Fig. 6 and S4). The highest SCO temperature was reached for x = 0.5 (with T_{SCO} = 226.3 K). As mentioned above, no alloy could be crystallized beyond this dopant concentration.

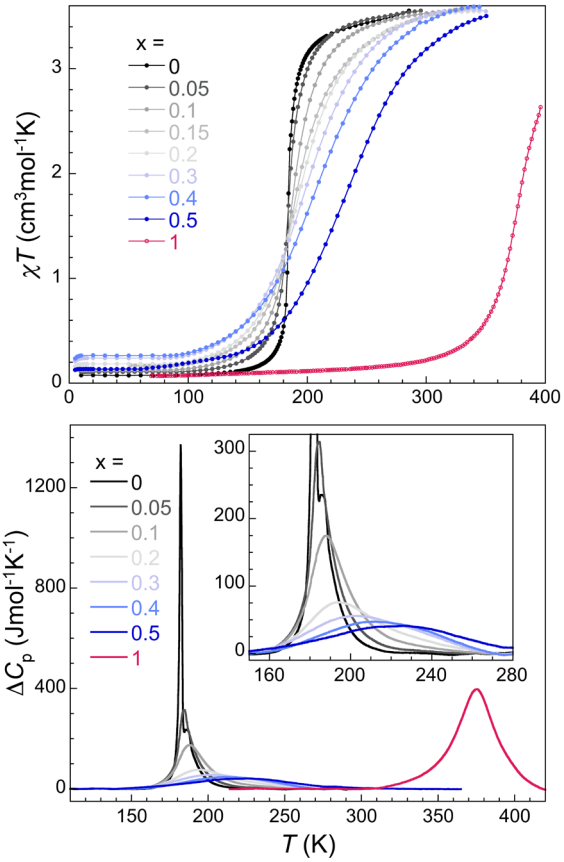

Figure 5. $\chi_M T$ *vs* T plots (top) and excess heat capacity (bottom) for the family of compounds $[Fe(Mebpp)_{2-2x}(Me2bpp)_{2x}](ClO_4)_2$ (**4***x*, see legend). The data for compounds **2** (x=0) and **3** (x=1)[69] are also included for reference.

The phase transitions of compounds **4***x* were also examined by differential scanning calorimetry (DSC, Fig. 5), and the results were consistent with the magnetic susceptibility measurements. Thus, in all cases, anomalies associated to the SCO phenomena were detected in the DSC. The maxima of the corresponding peaks shift to higher temperatures as x increases, as seen with the magnetic data. Fitting of the ΔC_p *vs.* T curves to Sorai's domain model[74,76] revealed smaller n values with increasing x (n being the number of centers per domain), confirming the loss of cooperativity caused by the doping (Fig. 7 and S5). This is in line with the evolution with x of the thermodynamic parameters, $\Delta_{SCO}S$ and $\Delta_{SCO}H$, obtained from the excess heat capacity ΔC_p (Fig. 6). While complex **2** experiences changes of entropy and enthalpy much larger than expected from the spin transition process only, suggesting a strong coupling of the system with phonons, this coupling, and thus the cooperativity diminishes as the dopant concentration grows. The variation of ΔT_{80} (temperature range needed to undergo an 80% conversion) with x (Fig. 7) also mirrors this decrease in cooperativity.

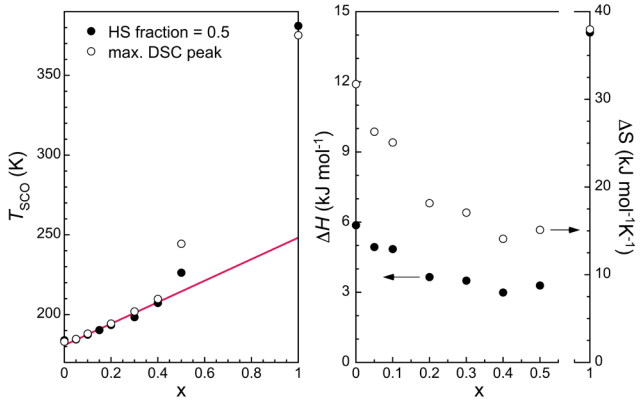

Figure 6. Variation of the SCO parameters, T_{SCO} and excess enthalpy $\Delta_{SCO}H$ and entropy $\Delta_{SCO}S$, as a function of x in compounds $[Fe(Mebpp)_{2-2x}(Me2bpp)_{2x}](ClO_4)_2$ (**4***x*). The data for compounds **2** (x=0) and **3** (x=1) are also included. The full red line is a linear dependence with T_{SCO} = 180.8 + 67.5x.

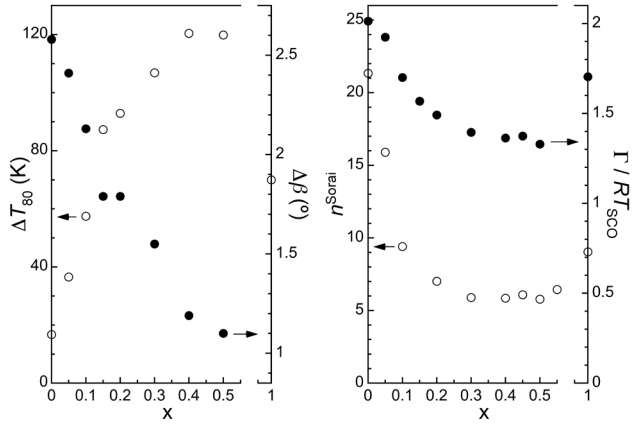

Figure 7.

Correlation Cooperativity-Structure

The extent to which the local structural effects of the SCO are translated into the lattice parameters has a direct impact on the cooperativity. The spin transition of various members of the $[Fe(Mebpp)_{2-2x}(Me2bpp)_{2x}](ClO_4)_2$ (**4***x*) family were analyzed in detail by variable temperature SCXRD. This study revealed that most cell parameters experience some significant changes in addition to these expected from the thermal variation, that can thus be ascribed to the SCO process (Figs. Sx and Sx). This is especially true for the unit cell angle β, which in all cases experiences a sharp change (by up to 2.5 %) upon SCO (Fig. 8 and S6). The decrease in cooperativity with increasing x can also be detected in this study, with more gradual thermal changes of the unit cell parameters, again in a particularly clear manner through the variation in β angle.

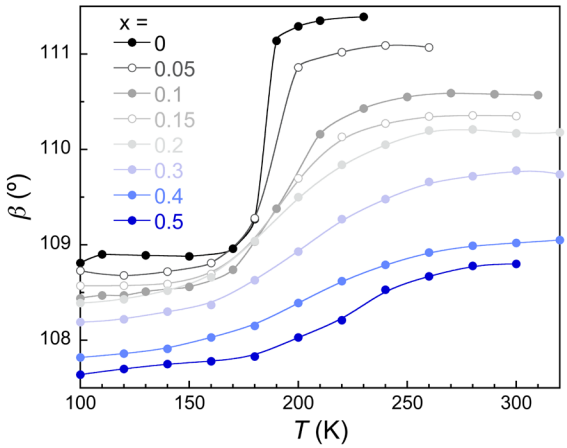

Figure 7. Temperature dependence of the monoclinic cell angle β upon the SCO process in compounds **2** and **4***x*.

Cooperativity changes within compounds $[Fe(Mebpp)_{2-2x}(Me2bpp)_{2x}](ClO_4)_2$ (**4***x*) are undoubtedly related to the modifications to the intermolecular interactions caused with the increase of *x*. Figure 9 shows the variation of average distances defining the main intermolecular interactions between complexes identified in the lattice of compounds **4***x* (Fig. 3), measured as $C_{pz}\cdots$centroid (for the CH$\cdots\pi$ contacts) or centroid$\cdots$centroid (for the $\pi\cdots\pi$ interactions) separations. In this figure, most parameters vary very slightly in one or the other direction. Overall, the inclusion of Me2bpp causes the decrease of three parameters, and a comparatively larger increase of three other parameters, especially the C–H$\cdots\pi$ interaction '5' (Fig. 3). Therefore, the increase of *x* causes in general a decrease of the intensity of the *average* intermolecular contacts. Most importantly, however, is that the additional methyl groups borne by the dopant Me2bpp ligands cause a local disruption of some intermolecular interactions exerting a more intense effect to the propagation of the elastic interactions than revealed by the average evolution shown in Fig. 9. This local disruption is most likely at the origin of the drastic decrease in cooperativity observed already for very small concentrations of dopant (Fig. 7 and Sx). From $x > 0.2$, the cooperativity becomes more stable towards composition changes. The effect of the doping is, in general, similar to that observed on systems doped with isostructural non-SCO complexes. However, the disruption of the propagation of elastic interactions in the latter is different than here. In the metal-doped systems the weakening of cooperativity is caused by the lack of structural transition of the non-active centers. In the current alloys, it is due to the interruption of some intermolecular interactions.

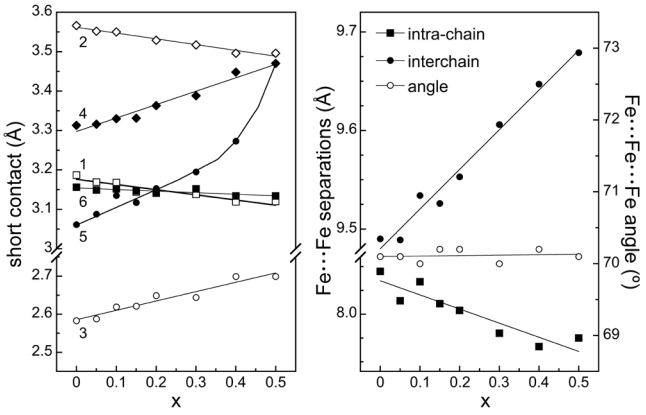

Figure 9. Variation with *x* of the distance parameters of the main intermolecular interactions between complexes and shortest Fe$\cdots$Fe separations within the isostructural lattice of compounds **2** and $[Fe(Mebpp)_{2-2x}(Me2bpp)_{2x}](ClO_4)_2$ (**4***x*).

Allosteric SCO

Another effect caused by the Me2bpp dopant of compounds **4***x* is the increase of T_{SCO} of the SCO. This increase, close to linear up to $x = 0.4$ ($T_{SCO} = 180.8 + 67.5x$) occurs at a completely different pace than the evolution of the cooperativity described above (Fig. 7), which suggests that the causes for the T_{SCO} dependence differ from these influencing the cooperativity. The increase of T_{SCO} with *x* must be explained from the fact that the SCO for $[Fe(Me2bpp)_2](ClO_4)_2$ (**3**) occurs at a higher temperature than for $[Fe(Mebpp)_2](ClO_4)_2$ (**2**). Indeed, T_{SCO} of **3** (378 K) was found to be much higher than that of **2** (184 K), but these were measured on lattices that are not isomorphic. While this precludes the comparison between both solids, it was also found that in solution, T_{SCO} (of **3**) > T_{SCO} (of **2**), although closer (232 and 281 K, respectively; ΔT_{SCO} = 49 K).[69] Part of the increase in T_{SCO} must therefore be ascribed to the effects caused by the additional methyl substituent, as previously reported for the pure complexes **2** and **3**.[69] This renders the increase of T_{SCO} with growing concentrations of Me2bpp analogous to that observed for the $Fe(Htrz)_{3-3x}(4\text{–}NH_2trz)_{3x}](ClO_4)_2$ system.[68] It must be noted however that compounds **4***x* are made of discrete complexes (not coordination polymers), therefore, one would expect to observe a SCO step for each of the three complexes present in the alloy. Since all the SCO curves feature a sole step, the increase in T_{SCO} must also involve the positive pressure induced on the $[Fe(Mebpp)_2]^{2+}$ complexes of the lattice by the other two species ($[Fe(Mebpp)(Me2bpp)]^{2+}$ and $[Fe(Me2bpp)_2]^{2+}$) expected to undergo SCO at higher temperature. Once the positive pressure is overcome, the SCO occurs in a concerted manner (at a lower temperature than expected for the species containing Me2bpp) as a result of an allosteric effect,[77] where the SCO of the $[Fe(Mebpp)_2]^{2+}$ centers induce the transition of the other two complexes present in the lattice. To the best of our knowledge, the SCO of Fe(II) complexes induced by an allosteric effect within the lattice has never been observed before.

CONCLUSIONS

The crystal lattice of complex $[Fe(Mebpp)_2](ClO_4)_2$ (**2**) is capable of admitting increasing amounts of ligand Me2bpp, leading to the formation of molecular alloys with composition $[Fe(Mebpp)_{2-2x}(Me2bpp)_{2x}](ClO_4)_2$ (**4***x*), only up to $x = 0.5$. The increase of *x* causes a decrease of the cooperativity of the SCO of this molecular system, noticed very suddenly for very low values of *x*. This is caused by the interruption of some intermolecular interactions due to the presence of the additional methyl substituent of the dopant ligand, and to gradual average changes to these interactions. The mean variation the intermolecular interaction parameters has been determined by SCXRD, to an unprecedented level of detail for SCO molecular alloys. The doping also causes an increase of the characteristic temperature of the spin transition. Following the previous information on the SCO temperatures of compounds $[Fe(Mebpp)_2](ClO_4)_2$ (**2**) and $[Fe(Me2bpp)_2](ClO_4)_2$ (**3**), it is concluded that this increase is the result of the chemical pressure caused by the presence in the lattice of species $[Fe(Mebpp)(Me2bpp)]^{2+}$ and $[Fe(Me2bpp)_2]^{2+}$, expected to have a higher T_{SCO}. In addition, the observation of a concerted, one step magnetic transitions for all compositions of the studied **4***x* alloys is most likely the result of a unique allosteric effect where the retarded SCO of the $[Fe(Mebpp)_2]^{2+}$ species, pushes the premature transitions of the other two species of the alloy.

ASSOCIATED CONTENT

Supporting Information

(Word Style "Section_Content"). A brief statement in nonsentence format listing the contents of material supplied as Supporting Information should be included, ending with “This material is available free of charge via the Internet at http://pubs.acs.org.”

AUTHOR INFORMATION

Corresponding Author

guillem.aromi@qi.ub.es
roubeau@unizar.es
Carlos.Bartual@uv.es

Present Addresses

¬ Instituto de Ciencia Molecular, Universidad de Valencia, Catedrático José Beltrán 2, 46980 Paterna, Spain.

Author Contributions

The manuscript was written through contributions of all authors. All authors have given approval to the final version of the manuscript.

Funding Sources

GA thanks the Generalitat de Catalunya for the prize ICREA Academia 2018 and QUANTERA for project SUMO (through PCI2018-093106). The authors acknowledge funding by the Spanish MINECO through CTQ2015-68370-P and PGC2018-098630-B-I00 (GA and CBM) and MAT2017-86826-R (OR). This research used resources of the Advanced Light Source, which is a DOE Office of Science User Facility under contract no. DE-AC02-05CH11231 (SJT).

Notes

The authors declare no competing financial interests.

ACKNOWLEDGMENT

(Word Style "Section_Content"). Generally the last paragraph of the paper is the place to acknowledge people (dedications), places, and financing (you may state grant numbers and sponsors here). Follow the journal’s guidelines on what to include in the Acknowledgement section.

ABBREVIATIONS

SCO, Spin crossover; HS, high spin; LS, low spin; MALDI-TOF, Matrix-Assisted Laser Desorption/Ionization – time of flight; MS, mass spectrometry; SCXRD, single crystal X-ray diffraction; PXRD, powder X-ray diffraction;DSC, differential scanning calorimetry.

REFERENCES

SYNOPSIS TOC (Word Style "SN_Synopsis_TOC"). If you are submitting your paper to a journal that requires a synopsis graphic and/or synopsis paragraph, see the Instructions for Authors on the journal's homepage for a description of what needs to be provided and for the size requirements of the artwork.

Insert Table of Contents Graphic and Synopsis Here

---

(1) Halcrow, M. A. *Spin-Crossover Materials: Properties and Applications*; Wiley: West Sussex, UK, 2013.

(2) Gütlich, P.; Goodwin, H. A. *Spin Crossover in Transition Metal Compounds I–III*; Springer: Berlin, 2004; Vol. 233-235.

(3) Gutlich, P.; Hauser, A.; Spiering, H. *Angew. Chem., Int. Ed.* **1994**, *33*, 2024-2054.

(4) Bousseksou, A.; Molnar, G.; Salmon, L.; Nicolazzi, W. *Chem. Soc. Rev.* **2011**, *40*, 3313-3335.

(5) Saha, S.; Stoddart, J. F. *Chem. Soc. Rev.* **2007**, *36*, 77-92.

(6) Bogani, L.; Wernsdorfer, W. *Nat. Mater.* **2008**, *7*, 179-186.

(7) Gamez, P.; Costa, J. S.; Quesada, M.; Aromí, G. *Dalton Trans.* **2009**, 7845-7853.

(8) Gütlich, P.; Gaspar, A. B.; Garcia, Y. *Beilstein J. Org. Chem.* **2013**, *9*, 342-391.

(9) Hogue, R. W.; Singh, S.; Brooker, S. *Chem. Soc. Rev.* **2018**, *47*, 7303-7338.

(10) Collet, E.; Guionneau, P. *C. R. Chim.* **2018**, *21*, 1133-1151.

(11) Bartual-Murgui, C.; Diego, R.; Vela, S.; Teat, S. J.; Roubeau, O.; Aromí, G. *Inorg. Chem.* **2018**, *57*, 11019-11026.

(12) Ortega-Villar, N.; Munoz, M. C.; Real, J. A. *Magnetochemistry* **2016**, *2*.

(13) Phonsri, W.; Davies, C. G.; Jameson, G. N. L.; Moubaraki, B.; Ward, J. S.; Kruger, P. E.; Chastanet, G.; Murray, K. S. *Chem. Commun.* **2017**, *53*, 1374-1377.

(14) Shatruk, M.; Phan, H.; Chrisostomo, B. A.; Suleimenova, A. *Coord. Chem. Rev.* **2015**, *289-290*, 62-73.

(15) Arcis-Castíllo, Z.; Zheng, S.; Siegler, M. A.; Roubeau, O.; Bedoui, S.; Bonnet, S. *Chem., Eur. J.* **2011**, *17*, 14826-14836.

(16) Halcrow, M. A. *Chem. Lett.* **2014**, *43*, 1178-1188.

(17) Halcrow, M. A. *Chem. Soc. Rev.* **2011**, *40*, 4119-4142.

(18) Bao, X.; Leng, J.-D.; Meng, Z.-S.; Lin, Z.; Tong, M.-L.; Nihei, M.; Oshio, H. *Chem., Eur. J.* **2010**, *16*, 6169-6174.

(19) Fujinami, T.; Nishi, K.; Matsumoto, N.; Iijima, S.; Halcrow, M. A.; Sunatsuki, Y.; Kojima, M. *Dalton Trans.* **2011**, *40*, 12301-12309.

(20) Yamada, M.; Ooidemizu, M.; Ikuta, Y.; Osa, S.; Matsumoto, N.; Iijima, S.; Kojima, M.; Dahan, F.; Tuchagues, J.-P. *Inorg. Chem.* **2003**, *42*, 8406-8416.

(21) Quesada, M.; Prins, F.; Bill, E.; Kooijman, H.; Gamez, P.; Roubeau, O.; Spek, A. L.; Haasnoot, J. G.; Reedijk, J. *Chem., Eur. J.* **2008**, *14*, 8486-8499.

(22) Knoll, C.; Muller, D.; Seifried, M.; Giester, G.; Welch, J. M.; Artner, W.; Hradil, K.; Reissner, M.; Weinberger, P. *Dalton Trans.* **2018**, *47*, 5553-5557.

(23) Craig, G. A.; Costa, J. S.; Roubeau, O.; Teat, S. J.; Aromi, G. *Chem., Eur. J.* **2012**, *18*, 11703-11715.

(24) Fumanal, M.; Jiménez-Grávalos, F.; Ribas-Arino, J.; Vela, S. *Inorg. Chem.* **2017**, *56*, 4474-4483.

(25) Roberts, T. D.; Tuna, F.; Malkin, T. L.; Kilner, C. A.; Halcrow, M. A. *Chem. Sci.* **2012**, *3*, 349-354.

(26) Halder, G. J.; Kepert, C. J.; Moubaraki, B.; Murray, K. S.; Cashion, J. D. *Science* **2002**, *298*, 1762.

(27) Quesada, M.; de la Pena-O'Shea, V. A.; Aromi, G.; Geremia, S.; Massera, C.; Roubeau, O.; Gamez, P.; Reedijk, J. *Adv. Mater.* **2007**, *19*, 1397-1402.
(28) Bonnet, S.; Molnár, G.; Sanchez Costa, J.; Siegler, M. A.; Spek, A. L.; Bousseksou, A.; Fu, W.-T.; Gamez, P.; Reedijk, J. *Chem. Mater.* **2009**, *21*, 1123-1136.
(29) Wei, R.-J.; Tao, J.; Huang, R.-B.; Zheng, L.-S. *Inorg. Chem.* **2011**, *50*, 8553-8564.
(30) Zhang, W.; Zhao, F.; Liu, T.; Yuan, M.; Wang, Z.-M.; Gao, S. *Inorg. Chem.* **2007**, *46*, 2541-2555.
(31) Sertphon, D.; Harding, P.; Murray, K.; Moubaraki, B.; Neville, S.; Liu, L.; Telfer, S.; Harding, D. *Crystals* **2019**, *9*, 116.
(32) Weber, B.; Kaps, E.; Weigand, J.; Carbonera, C.; Létard, J.-F.; Achterhold, K.; Parak, F. G. *Inorg. Chem.* **2008**, *47*, 487-496.
(33) Halcrow, M. A. *Coord. Chem. Rev.* **2009**, *253*, 2493-2514.
(34) Craig, G. A.; Roubeau, O.; Aromi, G. *Coord. Chem. Rev.* **2014**, *269*, 13-31.
(35) Elhaïk, J.; Money, V. A.; Barrett, S. A.; Kilner, C. A.; Evans, I. R.; Halcrow, M. A. *Dalton Trans.* **2003**, 2053-2060.
(36) Olguín, J.; Brooker, S. *Coord. Chem. Rev.* **2011**, *255*, 203-240.
(37) Bartual-Murgui, C.; Codina, C.; Roubeau, O.; Aromí, G. *Chem., Eur. J.* **2016**, *22*, 12767-12776.
(38) Tao, J.; Wei, R.-J.; Huang, R.-B.; Zheng, L.-S. *Chem. Soc. Rev.* **2012**, *41*, 703-737.
(39) Wei, R.-J.; Li, B.; Tao, J.; Huang, R.-B.; Zheng, L.-S.; Zheng, Z. *Inorg. Chem.* **2011**, *50*, 1170-1172.
(40) Bartual-Murgui, C.; Piñeiro-López, L.; Valverde-Muñoz, F. J.; Muñoz, M. C.; Seredyuk, M.; Real, J. A. *Inorg. Chem.* **2017**, *56*, 13535-13546.
(41) Miller, R. G.; Brooker, S. *Chem. Sci.* **2016**, *7*, 2501-2505.
(42) Valverde-Muñoz, F. J.; Seredyuk, M.; Meneses-Sánchez, M.; Muñoz, M. C.; Bartual-Murgui, C.; Real, J. A. *Chem. Sci.* **2019**, *10*, 3807-3816.
(43) Sorai, M.; Ensling, J.; Gütlich, P. *Chem. Phys.* **1976**, *18*, 199-209.
(44) Guetlich, P.; Link, R.; Steinhaeuser, H. G. *Inorg. Chem.* **1978**, *17*, 2509-2514.
(45) Haddad, M. S.; Federer, W. D.; Lynch, M. W.; Hendrickson, D. N. *J. Am. Chem. Soc.* **1980**, *102*, 1468-1470.
(46) Hauser, A.; Guetlich, P.; Spiering, H. *Inorg. Chem.* **1986**, *25*, 4245-4248.
(47) Martin, J.-P.; Zarembowitch, J.; Bousseksou, A.; Dworkin, A.; Haasnoot, J. G.; Varret, F. *Inorg. Chem.* **1994**, *33*, 6325-6333.
(48) Martin, J.-P.; Zarembowitch, J.; Dworkin, A.; Haasnoot, J. G.; Codjovi, E. *Inorg. Chem.* **1994**, *33*, 2617-2623.
(49) Janiak, C.; Scharmann, T. G.; Bräuniger, T.; Holubová, J.; Nádvorník, M. *Z. Anorg. Allg. Chem.* **1998**, *624*, 769-774.
(50) Chakraborty, P.; Enachescu, C.; Walder, C.; Bronisz, R.; Hauser, A. *Inorg. Chem.* **2012**, *51*, 9714-9722.
(51) Zheng, S.; Siegler, M. A.; Sánchez Costa, J.; Fu, W.-T.; Bonnet, S. *Eur. J. Inorg. Chem.* **2013**, *2013*, 1033-1042.
(52) Ganguli, P.; Guetlich, P.; Mueller, E. W. *Inorg. Chem.* **1982**, *21*, 3429-3433.
(53) Adler, P.; Wiehl, L.; Meibner, E.; Köhler, C. P.; Spiering, H.; Gütlich, P. *J. Phys. Chem. Solids* **1987**, *48*, 517-525.
(54) Sanner, I.; Meissner, E.; Ko¨ppen, H.; Spiering, H.; Gu¨tlich, P. *Chem. Phys.* **1984**, *86*, 227-233.
(55) Jakobi, R.; Spiering, H.; Wiehl, L.; Gmelin, E.; Guetlich, P. *Inorg. Chem.* **1988**, *27*, 1823-1827.
(56) Baldé, C.; Desplanches, C.; Gütlich, P.; Freysz, E.; Létard, J. F. *Inorg. Chim. Acta* **2008**, *361*, 3529-3533.
(57) Baldé, C.; Desplanches, C.; Wattiaux, A.; Guionneau, P.; Gütlich, P.; Létard, J.-F. *Dalton Trans.* **2008**, 2702-2707.
(58) Buchen, T.; Poganiuch, P.; Gütlich, P. *J. Chem. Soc., Dalton Trans.* **1994**, 2285-2288.

(59) Tayagaki, T.; Galet, A.; Molnár, G.; Muñoz, M. C.; Zwick, A.; Tanaka, K.; Real, J.-A.; Bousseksou, A. *The Journal of Physical Chemistry B* **2005**, *109*, 14859-14867.
(60) Tanasa, R.; Enachescu, C.; Stancu, A.; Varret, F.; Linares, J.; Codjovi, E. *Polyhedron* **2007**, *26*, 1820-1824.
(61) Baldé, C.; Desplanches, C.; Grunert, M.; Wei, Y.; Gütlich, P.; Létard, J.-F. *Eur. J. Inorg. Chem.* **2008**, *2008*, 5382-5389.
(62) Yu, Z.; Kuroda-Sowa, T.; Kume, H.; Okubo, T.; Maekawa, M.; Munakata, M. *Bull. Chem. Soc. Jpn.* **2009**, *82*, 333-337.
(63) Rotaru, A.; Dîrtu, M. M.; Enachescu, C.; Tanasa, R.; Linares, J.; Stancu, A.; Garcia, Y. *Polyhedron* **2009**, *28*, 2531-2536.
(64) Paradis, N.; Chastanet, G.; Létard, J.-F. *Eur. J. Inorg. Chem.* **2012**, *2012*, 3618-3624.
(65) Baldé, C.; Desplanches, C.; Le Gac, F.; Guionneau, P.; Létard, J.-F. *Dalton Trans.* **2014**, *43*, 7820-7829.
(66) Halcrow, M. A.; Chastanet, G. *Polyhedron* **2017**, *136*, 5-12.
(67) Sylla, M. S.; Baldé, C.; Daro, N.; Desplanches, C.; Marchivie, M.; Chastanet, G. *Eur. J. Inorg. Chem.* **2018**, *2018*, 297-304.
(68) Krober, J.; Codjovi, E.; Kahn, O.; Groliere, F.; Jay, C. *J. Am. Chem. Soc.* **1993**, *115*, 9810-9811.
(69) Bartual-Murgui, C.; Vela, S.; Darawsheh, M.; Diego, R.; Teat, S.; Roubeau, O.; Aromí, G. *Inorg. Chem. Front.* **2017**, *4*, 1374.
(70) Sheldrick, G. M., SAINT and SADABS, 2012, Bruker AXS Inc., Madison, Wisconsin, USA.
(71) Sheldrick, G. *Acta Cryst. A* **2015**, *71*, 3-8.
(72) Sheldrick, G. *Acta Cryst. C* **2015**, *71*, 3-8.
(73) Slichter, C. P.; Drickamer, H. G. *J. Chem. Phys.* **1972**, *56*, 2142-2160.
(74) Sorai, M.; Seki, S. *J. Phys. Chem. Solids* **1974**, *35*, 555-570.
(75) Sorai, M. *Top. Curr. Chem.* **2004**, *235*, 153-170.
(76) Sorai, M.; Nakazawa, Y.; Nakano, M.; Miyazaki, Y. *Chem. Rev.* **2013**, *113*, PR41-PR122.
(77) Tumanov, S. V.; Veber, S. L.; Greatorex, S.; Halcrow, M. A.; Fedin, M. V. *Inorg. Chem.* **2018**, *57*, 8709-8713.